Role of cervicitis in the Raman-based optical diagnosis of cervical intraepithelial neoplasia

Herculano da Silva Martinho
Universidade Federal do ABC-UFABC
Centro de Ciências Naturais e Humanas
09090-400, Santo André, São Paulo, Brazil
E-mail: herculano.martinho@ufabc.edu.br

Claudia Maria de Oliveira Monteiro da Silva
Maria Christina Botelho Mendonça Yassoyama
Patrícia de Oliveira Andrade
Renata Andrade Bitar
Ana Maria do Espírito Santo
Emilia Ângela Loschiavo Arisawa
Airton Abrahão Martin
Universidade do Vale do Paraíba-UniVap
Instituto de Pesquisa e Desenvolvimento
12244-000, São José dos Campos, São Paulo, Brazil

Abstract. The Raman-based optical diagnosis of normal cervix, inflammative cervix (cervicitis), and cervical intraepithelial neoplasia was investigated on samples of 63 patients. The main alterations were found in the 857 cm^{-1} (CCH deformation aromatic); 925 cm^{-1} (C–C stretching); $\sim$1247 cm^{-1} (CN stretch, NH bending of Amide III); 1370 cm^{-1} (CH$_2$ bending); and 1525 cm^{-1} (C=C/C=N stretching) vibrational bands in accordance with previously reported in the literature comparing normal and malignant cervical tissue. The statistical analysis (principal components analysis, clustering, and logistic regression models) applied to the spectral data indicated that the full discrimination among normal and neoplastic tissues of cervix by Raman optical biopsy is seriously affected by the presence of inflammatory infiltrates, which increases the false-positive rate. This fact is specially relevant once cervicitis is a very common state (noncancerous) of the cervix of sexually active woman. The results suggest that, for the correct Raman-based diagnosis of normal cervix from cervical intraepithelial neoplasia, it is necessary to use an auxiliary way to discriminate the contribution from the inflammatory infiltrates. © 2008 Society of Photo-Optical Instrumentation Engineers. [DOI: 10.1117/1.2976114]

Keywords: Optical biopsy; Raman spectroscopy; Cervical cancer.

1 Introduction

Cervical cancer is the second most common cancer among women worldwide, and it is generally more common in developing countries.[1] Each year, 471×10^3 new cases are reported and approximately 230×10^3 woman died due to this kind of cancer.[2]

The main causing agent is the sexually transmitted papilloma human virus (HPV).[3] Cervical malignancy is usually preceded by cervical intraepithelial neoplasia (CIN) of grades I, II, and III before becoming invasive.[3] It is widely known that a large amount of deaths by this pathology (estimated as $\sim$90%) would be avoided with early diagnosis.[3] This emphasizes the search for effective screening methods for cervix neoplasia.

The available screening and diagnosis methods (mainly Pap smear and colposcopy) have some shortcomings that make impossible fast, effective, and efficient supervision of cancer in the general population, mainly in developing countries. These limitations are due to the fact that all methods are based on subjective interpretations of morphological abnormalities. The cytological analysis of the cervix, which is the elementary principle of a Pap smear and colposcopy, for example, had a high false-negative rate of $\sim$50%.[4] This fact is inherent to the subjective histological grading of this pathology. It is common atypical cells be associated to inflammatory infiltrates and the slice be misinterpreted by the pathologist as simple cervix inflammation (cervicitis) instead of a malignance or neoplasia or vice versa. This high false-negative rate would limit the accuracy of screenings at very initial stages of the cervical cancer, which prevents an adequate treatment at this stage. As a consequence, a large number of patients will need a surgical procedure to remove the cancer that otherwise would have been detected and treated at the beginning.

Optical biopsy techniques, such as fluorescence spectroscopy,[5] polarized light scattering spectroscopy,[6] optical coherence tomography,[7] confocal reflectance microscopy,[8] and Raman spectroscopy[9–13] had been extensively used to characterize cervical cancers. In particular, the Raman spectroscopy technique was able to probe several biochemical alterations due to pathology development as a change in the DNA, glycogen, phospholipid, or noncollagenous proteins.[9–15]

All the above-cited studies claimed that the optical biopsy methods were able to discriminate normal and malignant tissues. However, to the best of our knowledge, no study presented in the literature concerned the influence of cervicitis on the optical diagnosis of cervix cancer. The objective of the present work is to cover this void, presenting a systematic study of normal, CIN I, and cervicitis cervical tissue by Fourier Transform (FT)–Raman spectroscopy.

2 Methodology

This research was carried out following the ethical principles established by the Brazilian Health Ministry and approved by

Address all correspondence to Herculano da Silva Martinho: Centro de Ciências Naturais e Humanas, Universidade Federal do ABC, Rua Catequese, 255-Santo André, São Paulo 09030-320 Brazil Tel: +55 11 4436-1859; Fax: +55 11 4436-1859; E-mail: hsmartinho@gmail.com

Table 1 Samples summary.

No. of samples	No. of spectra	Diagnosis
30	94	Normal
25	112	Cervicitis
8	24	CIN I

the local ethics in research committee (certificate 168/2004CEP–UniVap). Patients were informed concerning the subject of the research and gave their permission for the collection of tissue samples.

Cervix biopsies were collected from 63 patients. Thirty-three biopsies were collected from malignant sites (as indicated by Pap smear and colposcopy) and 30 from normal ones. Immediately after the procedure, the samples were identified, snap frozen and stored in liquid nitrogen (77 K) in cryogenic vials prior to FT-Raman spectra recording.

A FT-Raman spectrometer (Bruker RFS 100/S; Bruker Optics GmbH, Ettlingen, Germany) was used with an Nd:YAG laser at 1064 nm as the excitation light source. Laser power at the sample was maintained at 110 mW, while the resolution was set to 4 cm^{-1}. The spectra were recorded using 300 scans (nearly 10 min of acquisition time) with laser excitation done at the epithelial side of the tissues. For FT-Raman data collection, the samples were brought to room temperature and maintained moistened in 0.9% physiological solution to preserve their structural characteristics, then placed in a windowless aluminum holder for Raman spectra collection. Observation revealed that the chemical species in the physiological solution (Ca^{2+}, Na^+, K^+, Cl^-, water) presented no measurable Raman signal and their presence did not affect the tissue spectral signal. The typical size of samples was $3 \times 3 \times 1$ mm^3.

Typically, three to five Raman spectra were recorded on each sample, resulting in 230 spectra. Soon after the Raman measurements, the samples were fixed in 10% formaldehyde solution for further histopathological analysis. Each measured sample was histopathologically assessed by two pathologists. Details of all samples used in the study are shown in Table 1.

All spectra were baseline corrected and vector normalized. The typical baseline was a straight line in all cases. The algorithm used calculated the straight line, considering the first

and last experimental data points at 800 and 1800 cm^{-1}, respectively. The spectral differences were analyzed using multivariate principal components analysis (PCA). PCA was performed over the range 800–1800 cm^{-1} by computing the covariance matrix. The underlying data structure was summarized by clustering (*i*) the whole spectral data and (*ii*) PC2, PC3, and PC4 scores, both at 95% level of similarity using correlation distance measurement. The results were presented as a dendrogram. The set of PCs that provided the best classification after visual inspection of scattering plots were fed into the logistic regression (LR) algorithm[16] to determine the parameter equation that best differentiated the pathologic states. LR provides a method for modeling a binary 0 or 1) response variable and is based on the linear dependence between the logit function of the probability of response 1 and the parameters of diagnosis. In our case, these parameters are the PCs. Thus, the LR model equation is

$$\ln\left(\frac{p}{1-p}\right) = a + \sum_i b_i \mathrm{PC}_i, \qquad (1)$$

where p is the probability of obtaining response 1 and a and b_i are the model parameters.

For the LR modeling, data set was randomly divided into two independent portions (test and validation). The choice of spectra to be put into each set was made with the help a random-number-generator algorithm. The model's predictive ability was estimated by measuring the association between the response variable and predictive probabilities. The fit quality was tested by the deviance goodness of fit Pearson-χ^2 and Somer's D parameters. All these steps were performed with help of the statistical software Minitab, version 14.20 (Minitab Inc., State College, Pennsylvania, USA) and Mathematica 5.2 software (Wolfram Research, Champaign, IL, USA).

3 Results and Discussion

Figure 1 shows some typical histological stains representing normal [Fig. 1(a)], cervicitis [Fig. 1(b)], and CIN I [Fig. 1(c)] cervical tissues. The normal cervical tissues presented only discrete differences compatible with the expected biological variation. The cervicitis tissues were characterized as present-

Fig. 1 Histological stains representing (a) the normal (20x), (b) cervicitis (40x), and (c) CIN I (20x) cervix.
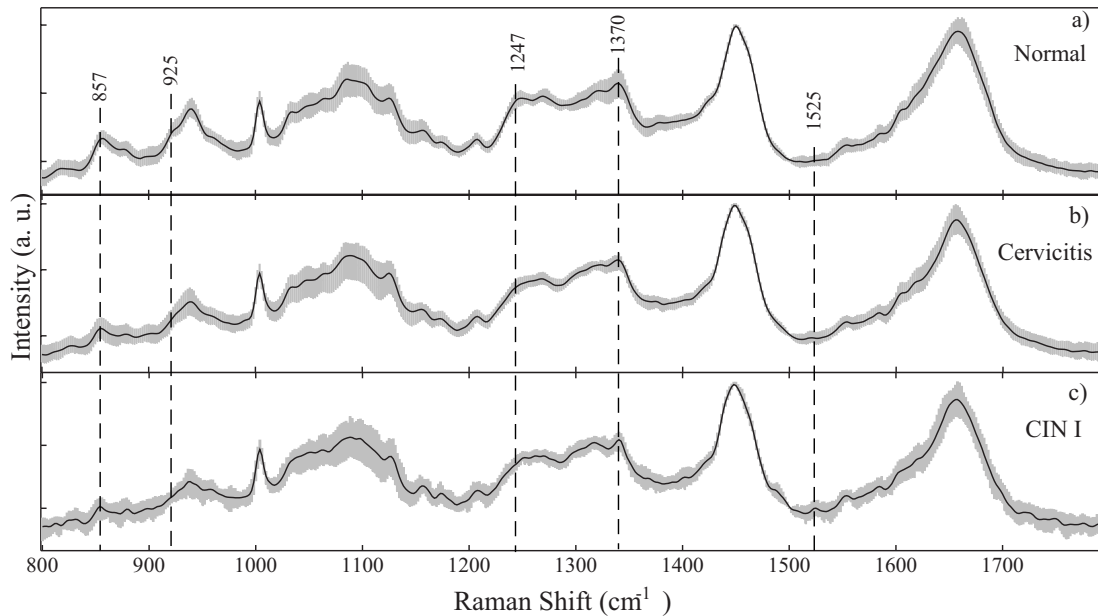
Fig. 2 Box plot that represents all cervix spectral data: (a) normal, (b) cervicitis, and (c) CIN I. Each spectrum was baseline corrected and vector normalized. The solid line is the mean Raman spectra. The vertical gray lines indicate the region between the first and third quartiles. The vertical dashed lines indicates the bands suffering the major alterations, as discussed in the text.

ing only inflammatory infiltrates without atypical cells while the CIN I presented both inflammatory characteristics and atypical cells.

The box plot of the spectral data is displayed in Fig. 2. The main spectral changes observed (when considering the interquartile region) were at 857 cm^{-1} (CCH deformation aromatic) 925 cm^{-1} (C-C stretching), ~1247 cm^{-1} (CN stretch, NH bending of Amide III), 1370 cm^{-1} (CH$_2$ bending), and 1525 cm^{-1} (C=C/C=N stretching) vibrational bands.

The 857 and 925 cm^{-1} bands were slightly more prominent on normal samples. These peaks are related to glycogen, as shown by Lyng et al.[10] As discussed by some works (e.g., Refs. 2, 10, 14, and 15), the decrease in these glycogen bands on malignant samples is an expected and observed fact. Glycogen is known to be linked to cellular maturation and disappears with loss of differentiation during neoplasia.[10]

The 1247 cm^{-1} Amide III band appeared slightly more prominent (~15% more intense) and well defined on normal samples. This was normally found on macro-Raman (laser spot ~100–200 μm) measurement setups.[9,11–13] The micro-Raman measurements of Lyng et al.[10] showed this spectral band ~50% more intense in malignant cervical epithelial cells than in normal ones. This opposite result could be justified by the Raman signal of the connective tissue, which is collagenrich. The micro-Raman setup is able to spatially discriminate connective, basal, or epithelial tissues cells. In fact, the spectra recorded from connective tissue of cervix (Fig.4(a) of Ref. 10) presented more intense 1247 cm^{-1} Amide III band than the basal or epithelial cells. The macromeasurement does not enable this kind of discrimination. However, because this signal is present in both normal and altered tissues, this will not influence on the spectral discrimination.

The other two bands at 1370 and 1525 cm^{-1} presented a slight intensity increase in the altered tissue when compared

to the normal one. These bands are related to nucleic acids, and similar intensity variation was also reported in the literature.[9–15]

Figure 3(a) presents the clustering of the spectral data using the whole (800–1800 cm^{-1}) spectra. The data are grouped into three clusters. The composition of each cluster is showed in Table 2. Cluster 1 is composed by samples diagnosed as normal (50%) and cervicitis (50%). Cluster 2 concentrates or almost all CIN I samples (20 samples from a total of 24 or 83% of them), but it was also composed of normal and cervicitis ones. Cluster 3 had the predominance of cervicitis samples (72%). Thus, the clustering indicated spectral mixing among normal, cervicitis, and CIN I tissues. To better discern about the similarity between samples and try to obtain a better discrimination, the PCA analysis was performed and the PC2 to PC4 principal components were clustered and showed on the dendrogram of [Fig. 3(b)]. Unfortunately, the clustering was essentially identical to the previous case [Fig. 3(a)].

The scattering plot of PC2–PC4 is shown in Fig. 4. There was some discrimination among the normal and CIN I data.

Table 2 Number of spectra per cluster.

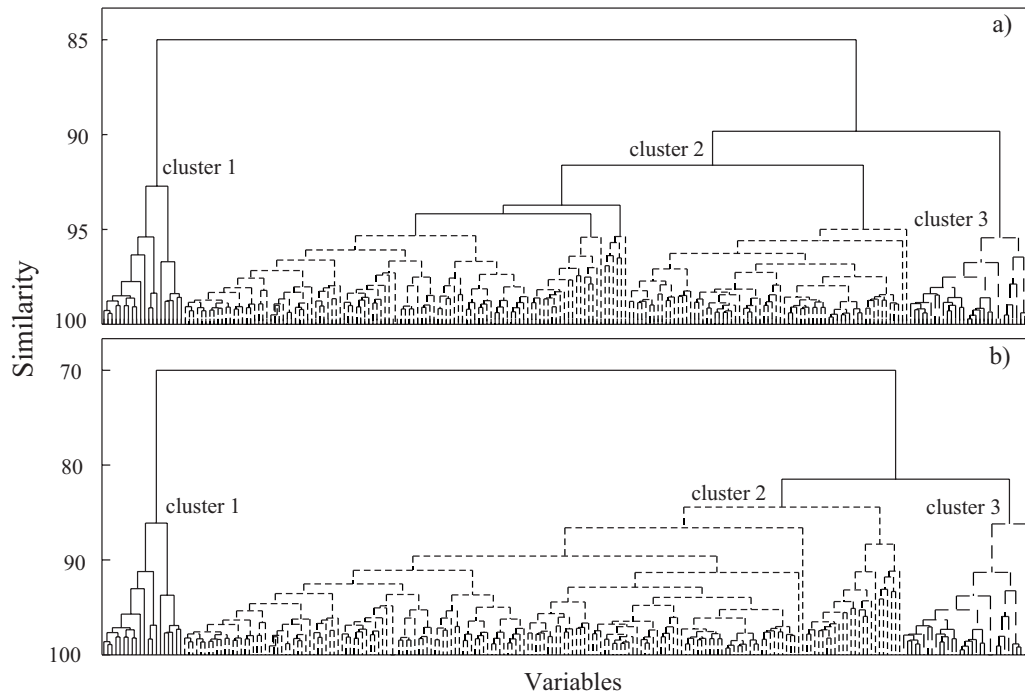| Diagnosis	Cluster 1	Cluster 2	Cluster 3	Total
Normal	10	79	5	94
Cervicitis	10	79	23	112
CIN I	—	20	4	24
Total	20	178	32	230

Fig. 3 Dendogram based on (a) the whole spectrum and (b) the PC2, PC3, and PC4 scores, showing the separation of the spectral data into three clusters (1, 2, and 3).

However, the cervicitis data points appeared to be in the midway among the normal and CIN I groups.

To quantify these findings, a nominal LR model was built, considering the three groups of samples. Compared was cervicitis to normal and CIN to normal, keeping the normal group as a reference. After fitting the model to a test set of spectra, it was applied to the validation set. The Pearson-χ^2 parameter for this model was found to be 0.633, indicating a poor goodness of fit. The Somer's D parameter was 0.79, implying a relatively low predictive ability of the model.

The LR was also applied to another situation considering two set of data: normal and altered (cervicitis and CIN I). The best fit to the test set was found to be a combination of PC3 and PC4 (Fig. 5)

$$\ln\left(\frac{p}{1-p}\right) = 0.6666 - 13.98\text{PC3} + 29.25\text{PC4}. \qquad (2)$$

After validation, the Pearson-χ^2 parameter for this model was found to be exactly 1, indicating a very good fit. The
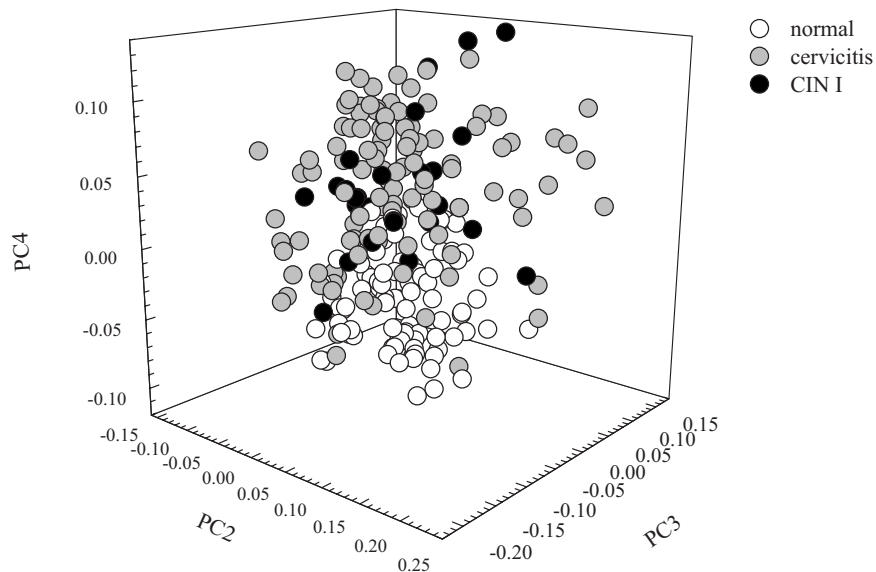

Fig. 4 Scattering plot of PC2–PC4 for the normal (open circle), CIN I (solid cyan circle), and cervicitis (solid black circle).
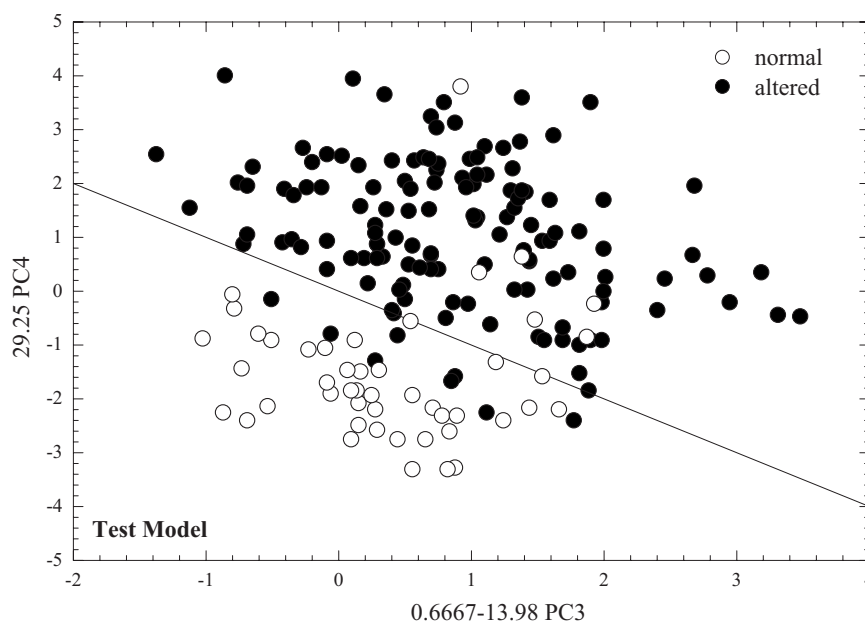
Fig. 5 Scattering plot for the best fitted LR model $\ln[p/(1-p)]=0.6666-13.98PC3+29.25PC4$. The solid line is a diagnosis line given by the $p=0.50$.

Somer's D parameter was 0.92, which means a high predictive ability of the model. The sensibility was found to be 93% and the specificity 85%. In spite of the high quality of the diagnosis model, this indicated a misclassification of cervicitis samples, which were intrinsically identified as CIN I neoplasia. In some sense, this is a similar situation to the conventional screening methods, where infiltrate inflammatory cells present in both cervicitis and CIN induce the wrong diagnostic. This implies that at this stage, the diagnosis by Raman will not provide substantial improvement in the screening power of cervix diseases because, in all kinds of malignance, there will be present inflammatory cells and some kind of cervicitis. At a worst-case situation, a nonmalignant cervicitis state (normal tissue with some inflammatory infiltrates) would be misclassified as CIN I, which is a very undesirable result.

4 Conclusions

The results presented in this work indicated that the full discrimination among normal and neoplastic CIN I tissues of cervix by Raman optical biopsy was seriously compromised by the presence of inflammatory infiltrates. In fact, both the crude biochemical analysis obtained by direct spectral comparison among normal, cervicitis, and CIN I samples; the clustering procedure; and the LR diagnosis model results indicated that the cervicitis samples were always misclassified as CIN I. This fact increases the false-positive rate of a Raman-based diagnosis. This is specially relevant because cervix inflammation is very common (noncancerous) disease of cervix. Thus, the results suggest that, for a safe and useful optical diagnosis of the cervix, it is mandatory find out a cervicitis-marker-like signal that could be found [e.g., by coupling an auxiliary technique (fluorescence, dichroism, etc.) to the Raman-based one].

References

1. D. Parkin, F. Bray, J. Ferlay, and P. Pisani, "Cancer Statistics, 2002," *Ca-Cancer J. Clin.* **55**(2), 74–108 (2005).
2. S. Neviliappan, L. F. Kan, T. T. L. Walter, S. Arulkumaran, and P. T. T. Wong, "Features of exfoliated cervical cells, cervical adenocarcinoma tissue, and an adenocarcinoma cell line (SiSo)," *Gynecol. Oncol.* **85**(1), 170–174 (2002).
3. M. H. Beers, and R. Berkow, *The Merck Manual*, 2nd ed., Lippincott Willians and Wilkins, New York (2005).
4. K. Nanda, D. McCrory, E. Myers, L. Bastian, V. Hasselblad, J. Hickey, and D. Matchar, "Accuracy of the Papanicolaou test in screening for and follow up of cervical cytologic abnormalities: A systematic review," *Ann. Intern Med.* **132**(10), 810–819 (2000).
5. S. Chang, I. Pavlova, N. Marin, M. Follen, and R. Richards-Kortum, "Fluorescence spectroscopy as a diagnostic tool for detecting cervical pre-cancer star, open," *Gynecol. Oncol.* **99**(3 Suppl. 1), S61–S63 (2005).
6. R. Gurjar, V. Backman, L. Perelman, I. Georgakoudi, K. Badizadegan, I. Itzkan, R. Dasari, and M. Feld, "Imaging human epithelial properties with polarized light-scattering spectroscopy," *Nat. Med.* **7**(11), 1245–1248 (2001).
7. P. Escobar, J. Belinson, A. White, N. Shakhova, F. Feldchtein, M. Kareta, and N. Gladkova, "Diagnostic eficacy of optical coherence tomography in the management of preinvasive and invasive cancer of uterine cervix and vulva," *Int. J. of Gynecol. Cancer* **14**(3), 470–474 (2004).
8. K. Carlson, I. Pavlova, T. Collier, M. Descour, M. Follen, and R. Richards-Kortum, "Confocal microscopy: Imaging cervical precancerous lesions," *Gynecol. Oncol.* **99**(3), S84–S88 (2005).
9. C. Krishna, N. Prathima, R. Malini, B. Vadhiraja, R. Bhatt, D. Fernandes, P. Kushtagi, M. Vidyasagar, and V. Kartha, "Raman spectroscopy studies for diagnosis of cancers in human uterine cervix" *Vib. Spectrosc.* **41**(1), 136–141 (2006).

10. F. Lyng, E. Faoláin, J. Conroy, A. Meade, P. Knief, B. Duffy, M. Hunter, J. Byrne, P. Kelehan, and H. Byrne, "Vibrational spectroscopy for cervical cancer pathology, from biochemical analysis to diagnostic tool," *Exp. Mol. Pathol.* **82**(2), 121129 (2007).

11. U. Utzinger, D. Heintzelman, A. Mahadevan-Jansen, A. Malpica, M. Follen, and R. Richards-Kortum, "Near-infrared Raman spectroscopy for in vivo detection of cervical precancers," *Appl. Spectrosc.* **55**(8), 955–959 (2001).

12. A. Mahadevan-Jansen, M. Mitchell, N. Ramanujam, U. Utzinger, and R. Richards-Kortum, "Development of a fiber optic probe to measure NIR Raman spectra of cervical tissue *in vivo*," *Photochem. Photobiol.* **68**(3), 427–431 (1998).

13. A. Mahadevan-Jansen, M. Mitchell, N. Ramanujam, A. Malpica, S. Thomsen, U. Utzinger, and R. Richards-Kortum, "Near-infrared Raman spectroscopy for *in vitro* detection of cervical precancers," *Photochem. Photobiol.* **68**(1), 123–132 (1998).

14. S. J. Millera, R. M. Lavkerb, and T.-T. Sunc, "Interpreting epithelial cancer biology in the context of stem cells: Tumor properties and therapeutic implications," *Biochim. Biophys. Acta Rev. Cancer* **1756**, 25–52 (2005).

15. N. Stone, C. Kendall, N. Shepherd, P. Crow, and H. Barr, "Near-infrared Raman spectroscopy for the classification of epithelial precancers and cancers," *J. Raman Spectrosc.* **33**, 564–573 (2002).

16. V. Bewick, L. Cheek, and J. Ball, "Statistics review 14: Logistic regression," *J. Crit. Care* **9**, 112–118 (2005).